

# Biomimetic Monolayer and Bilayer Membranes Made From Amphiphilic Block Copolymer Micelles

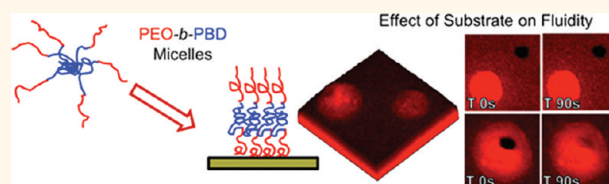
Matthew P. Goertz,\* Lauryn E. Marks, and Gabriel A. Montaño\*

Center for Integrated Nanotechnologies, Los Alamos National Laboratories, Los Alamos, New Mexico 87545, United States

**B**iomimetic membranes are commonly used to gain knowledge of fundamental biological processes and as biomaterials in devices due to their inherent biocompatibility and ability to host biomolecules.<sup>1</sup> Though these membranes are traditionally created with naturally occurring lipids, amphiphilic block copolymers can also be used as synthetic analogues of lipids to create membrane-based nanocomposite materials.<sup>2</sup> Through simple variation of polymer molecular weight (MW), composition, and structure (*i.e.*, diblock, triblock, branched), it is possible to vary several membrane properties. It is known that lateral diffusivity, thickness, elastic properties, and permittivity may be controlled over a broader range than can be achieved with lipid systems.<sup>2</sup> While there is a wealth of knowledge available on polymer vesicles<sup>2–4</sup> (aka polymersomes) and micelles,<sup>5</sup> relatively little is known about supported thin films of these polymer assemblies.

Understanding the fundamental interactions that dictate membrane properties is crucial to our ability to design biomimetic membrane architectures that, like biology, effectively seek to tune properties of membrane-bound molecules *via* the scaffold instead of by complex molecular functionalization. Specifically, the ability to control biomembrane architectures and incorporate molecules that mimic complex biological function is beginning to be realized. It was recently demonstrated that amphiphilic polymer vesicles could be deposited into a solid surface to create supported membrane architectures.<sup>6–10</sup> These initial studies have elucidated mechanisms of vesicle fusion, probed membrane topography, and resistance to drying instabilities. However, several questions regarding the properties of supported block copolymer membranes remain unanswered.

## ABSTRACT



The deposition of amphiphilic poly(ethylene oxide)-*block*-poly(butadiene) (PEO-*b*-PBD) copolymer micelles is demonstrated on solid substrates. Depending upon surface chemistry, micelle adsorption creates either monolayer or bilayer films. Lateral diffusion measurements reveal that strong coupling between hydrophilic surfaces and PEO blocks creates immobile bilayers, while monolayers retain the fluidity previously observed in vesicular assemblies.

**KEYWORDS:** polymer adsorption · biomimetic membranes · self-assembly · block copolymers · micelles · surfactants

Foremost of these questions is investigating if supported membranes retain the lateral diffusivity/fluidity that is observed in vesicular assemblies. Maintaining fluidity is of paramount importance in designing responsive biomimicking composite materials. Specifically, fluidity allows membrane-bound species to translocate in their host matrix and interact with molecules other than their nearest neighbors. Additionally, we are interested in combining the concept of polymer-based membranes with the established field of polymer/surfactant micelle adsorption.<sup>5,11–15</sup> Though previous work has utilized vesicle forming polymers to create supported membranes, micelle adsorption can also be used to create membranes for adaptive materials. In fact, block copolymer adsorption has been used for nearly 30 years to create surfaces with specific wetting, dispersion, and biocompatibility qualities.<sup>5,16</sup>

In this work, we demonstrate that deposition of short chain poly(ethylene oxide)-*block*-poly(butadiene) (PEO-*b*-PBD) micelles is effective at creating biomimetic membranes that

\* Address correspondence to mgoertz@lanl.gov, gbmon@lanl.gov.

Received for review November 18, 2011 and accepted January 17, 2012.

Published online January 17, 2012  
10.1021/nn204491q

© 2012 American Chemical Society

are defect-free over several hundred square micrometers. The PEO functionality was specifically chosen for its inherent biocompatibility and nonbiofouling properties when bound to surfaces.<sup>17</sup> Through an exhaustive microscopy effort, we have characterized topography, lateral diffusivity, thickness, and stability of membranes made by fusion of polymer micelles to solid supports. Depending upon surface chemistry, we find that micelles can be made to organize on surfaces as either monolayers or bilayers. While the monolayers display lateral fluidity, transport in bilayer is inhibited. This is most likely due to strong coupling between the substrate and adsorbed polymer.

## RESULTS AND DISCUSSION

**Characterization of Micelles.** The size of PEO-*b*-PBD aggregates was analyzed through dynamic light scattering (DLS) (Figure 1). Figure 1A reveals that the roughly equivalent weight fraction of PEO to PBD used in our study produces aggregates with a number average hydrodynamic radius ( $R_h$ ) of 6 nm. The size of these aggregates suggests that these polymers form micelles instead of larger structures such as vesicles. This result agrees with the “rule of thumb” that amphiphilic polymers with hydrophilic/hydrophobic weight fractions of  $\sim 0.5$  produce micelles, while lower fractions produce worm-like micelles and vesicles.<sup>2</sup> Micelle formation at equal weight fraction occurs because hydration of PEO causes swelling and an effective volume increase versus PBD. The swelling creates cone-shaped polymer chains that pack into micelles, effectively burying the PBD core and shielding it from water. The surface area and volume weighted  $R_h$  were found to be 8 and 30 nm, respectively. These higher order averages are more influenced by larger particles and indicate the presence of larger polymer aggregates in solution. Aggregation is most likely due to localized heating during the sonication necessary to dissolve the polymer in water. This is demonstrated through the irreversible cloud point shown in Figure 1B. As the micelle solution is heated, the turbidity dramatically increases between 50 and 70 °C; upon cooling to room temperature and reheating a second time, no change in turbidity is observed. This is interpreted as irreversible aggregation of micelles during heating. This aggregation necessitates temperature control during micelle formation, which is accomplished here through sonication in an ice bath.

**Adsorption on Surfaces.** The adsorption of PEO-*b*-PBD micelles was characterized through QCM, AFM, and fluorescence microscopy (Figures 2–4). The combination of microbalance and microscopy techniques allows us to probe the adsorption kinetics, adsorbed mass, topography, and lateral diffusion characteristics of deposited films from the nano to microscale. Figure 2

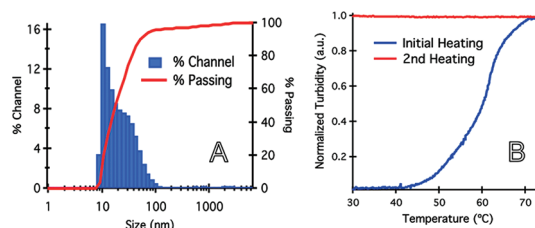


Figure 1. Dynamic light scattering (A) and cloud point determination (B) of PEO-*b*-PBD micelles. Dynamic light scattering data are displayed as the percentage of total particles within a specific size (diameter) channel (left, blue) and as the percentage of particles passing below a specific size (right, red). Turbidity data are normalized to the maximum amount of scattered light during the first heating and plotted versus solution temperature. The solution was initially heated to 75 °C (blue), cooled to room temperature, and reheated (red).

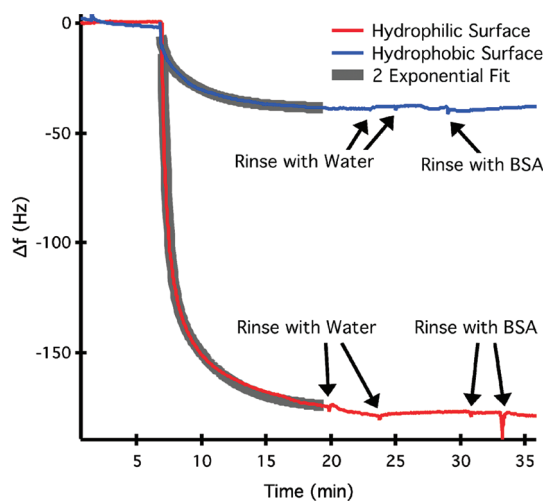


Figure 2. Quartz crystal microbalance results of PEO-*b*-PBD micelles deposited on hydrophilic (red) and hydrophobic (blue) borosilicate-coated quartz resonator sensors. The change in the third harmonic of the resonant frequency is plotted versus time. A fit to the two exponential decay model described in the text is shown in gray.

shows the change in resonant frequency of a QCM sensor as its surface is exposed to a 1 mg/mL solution of PEO-*b*-PBD micelles. The sensor is initially equilibrated with water followed by injection of polymer at  $\sim 7$  min. For QCM surfaces with either hydrophilic or hydrophobic surfaces, we observe an immediate decrease in the sensor's resonant frequency that decays to a stable value in  $\sim 15$  min. The change in resonant frequency ( $\Delta f$ ) is related to the change in mass ( $\Delta m$ ) for the quartz resonator sensor through the Sauerbrey equation.<sup>18</sup> In its simplest form, this relationship is  $\Delta f = -a\Delta m$ , where  $a$  is an instrument constant. Therefore, Figure 2 shows that the asymptotic frequency change and total mass of adsorbed material is  $\sim 3\times$  for adsorption on hydrophilic surfaces, compared to a hydrophobic substrate. The stability against rinsing and resistance to biofouling of adsorbed films was tested by washing the surfaces first with water and then a 50  $\mu\text{g/mL}$  aqueous solution of bovine serum albumin

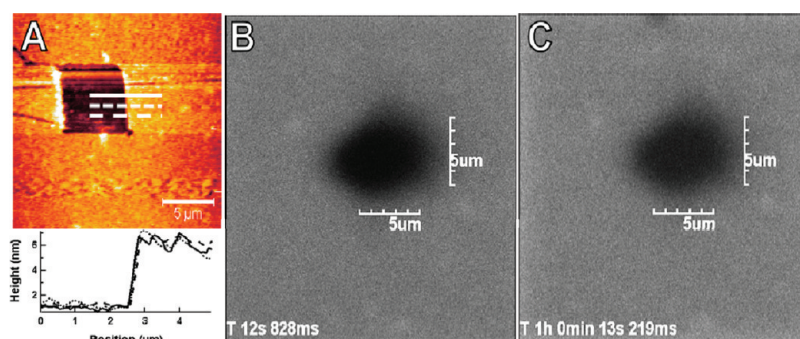


Figure 3. AFM (A) and fluorescence microscopy (B,C) images taken of PEO-*b*-PBD micelles deposited on hydrophilic glass. AFM image shows the topography after removing a section of the polymer film through scratching. Line scans of the three locations marked with white lines are shown below the image. Fluorescence microscopy images using fluorescein-labeled PEO-*b*-PBD as a contrast agent depict the lack of recovery during a FRAP measurement taken 12 s (B) and 1 h (C) after photobleaching. Scale bar represents 5  $\mu\text{m}$  for all images.

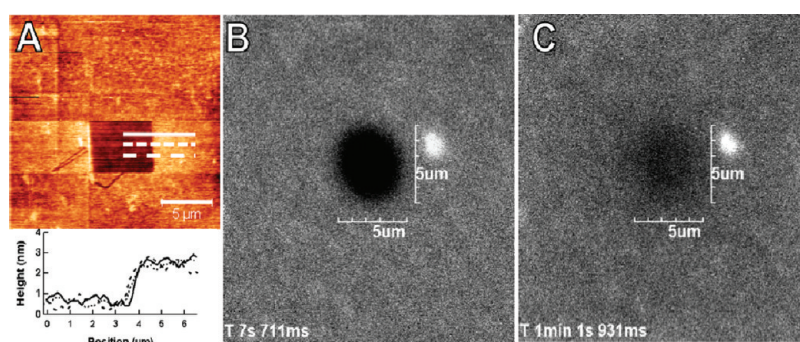


Figure 4. AFM (A) and fluorescence microscopy (B,C) images taken of PEO-*b*-PBD micelles deposited on hydrophobic glass. AFM image shows the topography after removing a section of the polymer film through scratching. Line scans of the three locations marked with white lines are shown below the image. Fluorescence microscopy images using fluorescein-labeled PEO-*b*-PBD as a contrast agent depict near-complete recovery during a FRAP measurement taken 7 s (B) and 1 min (C) after photobleaching. Scale bar represents 5  $\mu\text{m}$  for all images.

(BSA). Figure 2 demonstrates that washing with either of these solutions produces only transient changes and no discernible net change in adsorbed mass. The kinetics of polymer adsorption was analyzed by fitting the data in Figure 2 to an exponential decay model. Similar to previous micelle adsorption studies, we found that a two-component exponential model was needed to accurately fit our data.<sup>19</sup> Fits shown in Figure 2 are used to find the final resonant frequency ( $f_{\text{final}}$ ) of the sensor along with the amplitude ( $A$ ) and decay time constant ( $\tau$ ) for each fit component according to  $\Delta f = f_{\text{final}} + A_1 \exp(-t/\tau_1) + A_2 \exp(-t/\tau_2)$ . Averaging three adsorption experiments produces the results shown in Table 1.

AFM images shown in Figure 3A reveal that deposition of micelles onto hydrophilic glass produces a defect-free film over several square micrometers. Further imaging over both larger and smaller scales (shown in Supporting Information) reveals similar defect-free films from the molecular level up to several hundred square micrometers. Roughness values measured using AFM varied between samples and averaged  $\sim 1.5$  nm. Note that, using our cleaning protocol, glass coverslips display a roughness of  $< 0.5$  nm. Using the sharp AFM tip to scratch off the film and reveal the underlying glass substrate allows us to measure the

**TABLE 1. Results of Fitting QCM Data of Micelle Adsorption Using a Two-Component Exponential Decay Model (Averages of Three Runs  $\pm$  Standard Deviation Are Reported)**

surface chemistry	$f_{\text{final}}$ (Hz)	$A_1$ (Hz)	$\tau_1$ (s)	$A_2$ (Hz)	$\tau_2$ (s)
hydrophilic	$170 \pm 5$	$101 \pm 11$	$24 \pm 6$	$60 \pm 3$	$210 \pm 21$
hydrophobic	$45 \pm 3$	$9 \pm 2$	$18 \pm 4$	$24 \pm 5$	$186 \pm 17$

thickness of the polymer film. The three line scans shown in Figure 3A indicate that the polymer film is  $\sim 5$  nm thick. Note that this image was acquired using the lightest possible “tapping” amplitude capable of producing quality images (set point of  $\sim 90\%$  vs free oscillation). This condition is necessary to avoid height artifacts due to compression of the polymer from the AFM tip.

The fluorescence microscopy images shown in Figure 3 also indicate our ability to create defect-free films over many square micrometers. Through addition of fluorescently labeled PEO-*b*-PBD or fluorescent lipid molecules, we observe uniform intensity images that correspond to homogeneous dye incorporation throughout the polymer film. Fluorescent probes also allow for characterization of the lateral diffusion through fluorescence recovery after photobleaching

(FRAP) measurements.<sup>20</sup> Lateral diffusion of both the polymer and the incorporated lipid–dye moieties was determined. For polymer diffusion, fluorescein conjugated to PEO-*b*-PBD was used as a direct reporter. Lipid-based dyes were also incorporated into the polymer micelles and used as a probe for determination of diffusion of small molecules in the polymer membrane. The FRAP measurement in Figure 3 shows that, for the smallest bleach spot attainable with our microscope, fluorescently labeled PEO-*b*-PBD displayed no recovery over a period of 1 h on the hydrophilic substrate. Similar results were obtained using both C<sub>12</sub>-Bodipy-PC and Texas Red DHPE lipid-based dyes. Though this does not indicate a complete lack of fluidity, we can determine the maximum diffusion constant ( $D$ ) accessible in our experimental time frame. The half-life for recovery ( $\tau_{1/2} = 0.22R^2/D$ ), that is, when fluorescence intensity returns to half of its pre-bleach value, is  $\tau_{1/2} = 0.22R^2/D$ , where  $R$  is the radius of the bleached spot.<sup>21</sup> Accordingly, for a 2.5  $\mu\text{m}$  radius bleach spot, the half-life was not reached in 1 h. Therefore, the diffusion constant is smaller than  $4 \times 10^{-4} \mu\text{m}^2/\text{s}$ .

The effect of surface chemistry on the deposition of PEO-*b*-PBD micelles was investigated through deposition on a hydrophobically modified glass substrate. Figure 4 shows a combination of AFM and fluorescence microscopy of PEO-*b*-PBD deposited on an octylsilane self-assembled monolayer (SAM). While we observe that the general topography, roughness, and defect-free nature of polymer films remains very similar to deposition on hydrophilic glass, the thickness and lateral diffusivity are changed. Using the AFM tip to remove a portion of the polymer film and reimaging reveals that the polymer film is  $\sim 2.5$  nm thick, about half that for the same material on hydrophilic glass. Also noticeably different is the recovery observed during FRAP experiments. We observe that, for the same bleach spot used in Figure 3, we now observe near-complete recovery within 1 min. Repeating this experiment on multiple samples with bleach spot radii from 2.5 to 50  $\mu\text{m}$ , the self-diffusion constant is found to be  $0.15 \pm 0.07 \mu\text{m}^2/\text{s}$  with a mobile fraction of  $\sim 90$ –100%. This diffusion coefficient is at least  $10^3$  times larger than for depositions on hydrophilic surfaces. Similar results were obtained using both lipid-based dyes. Before considering the differences in fluid properties between depositions on these two surfaces, we must first construct a model for how PEO-*b*-PBD micelles adsorb into thin films. Combining the data presented in Figures 2–4 can create such a model.

Adsorption of micelles from a selective solvent typically occurs through two possible mechanisms, adsorption of either individual molecules or intact micelles.<sup>5,15,22</sup> Following adsorption, surface-bound polymers can rearrange into a variety of structure including highly organized periodic films of micelles and multilayers. The two-step adsorption kinetics

observed in Figure 2 suggests that PEO-*b*-PBD micelles and individual chains adsorb simultaneously, each with a distinct time scale. While it is unclear which time scale corresponds to each adsorption pathway, the amplitudes in Table 1 show that the relative magnitude of each adsorption mechanism is dependent on substrate chemistry. Recalling that micelles have a diameter of 12 nm and that AFM imaging produced a film with nanometer level uniformity, our measured films thicknesses of 5 and 2.5 nm exclude the possibility of intact micelles bound to the surfaces. In the absence of surface-bound micelles, the two-step adsorption kinetics observed in Figure 2 suggests that PEO-*b*-PBD chains and micelles first adsorb and then rearrange to adapt a thin film geometry with chains either lying down (parallel) or standing up (perpendicular) relative to the substrate. These two conformations can be distinguished through several observations. First, if the polymer chains were lying down at a homogeneous surface coverage, we expect a constant film thickness independent of the substrate. Second, the nonmixing behavior between PEO and PBD induces phase separation that should be detectable through microscopy for chains lying flat on a substrate. When dispersed in water, this phase separation is demonstrated by the formation of assemblies such as micelles, and similar phase separation is expected in thin films of nonmixing polymers. If the PEO-*b*-PBD chains lie flat with respect to a substrate, the equal weight fraction blocks would most likely create phase separation in the form of a striped pattern that should be visible through AFM imaging. Furthermore, the observation in Figure 2 that on either surface chemistry films of adsorbed PEO-*b*-PBD resist adsorption of BSA indicates that PEO is preferentially exposed to water. Bovine serum albumin is a small protein that is known to adsorb to glass and hydrophobic surfaces and is repelled by hydrophilic polymer brushes such as PEO.<sup>23</sup> These observations indicate that PEO-*b*-PBD micelle deposition leads to the creation of chains standing up on both substrates, creating densely packed bilayers on hydrophilic glass and monolayers on hydrophobic surfaces. Each monolayer is  $\sim 2.5$  nm thick, and we expect lamellar phase separation in the plane of the substrate. Similar to supported lipid bilayers, the hydrophobic PBD blocks most likely form a buried interface to minimize their interaction with water. A schematic of the proposed model is shown in Figure 5. As shown in Figure 2, the QCM results indicate that copolymer bilayers have  $\sim 3\times$  the mass of monolayers. This is most likely due either denser packing of polymer chains into bilayers or water of hydration that is entrapped in or under the bottom leaflet of the bilayer.<sup>24–26</sup> While fusion of lipid vesicles onto hydrophilic and hydrophobic surfaces is well-known to create similar bilayers and monolayers,<sup>27,28</sup> this is the first demonstration of a similar phenomenon for block copolymer micelles.

Deposition of micelles on a surface patterned with regions of hydrophilic and hydrophobic functionality allows us to further verify the conformation of surface-bound polymer chains. Accordingly, we deposited PEO-*b*-PBD micelles on silicon wafers patterned through microcontact printing with a hydrophobic octadecylsilane SAM. Surfaces were characterized through scanning imaging ellipsometry and AFM before (Figure 6A,C) and after micelle deposition (Figure 6B,D). These images show  $20 \times 20 \mu\text{m}$  squares of a SAM that are  $\sim 2.5$  nm above the silicon substrate. Scanning ellipsometry reveals that after micelle deposition the surface is covered with a homogeneous film with an average thickness of 5.2 nm. This agrees with our theory that PEO-*b*-PBD micelles adsorb to make monolayers that are roughly 2.5 nm thick on hydrophobic surfaces and 5 nm thick bilayers on hydrophilic glass or, in this case, native oxide terminated silicon. Similarly, AFM images show that the distinct boundary of the SAM-stamped regions is diminished upon micelle deposition. Line scan analysis of Figure 6D shows that stamped and unstamped regions have roughly similar heights, though roughness near the stamp boundary remains.

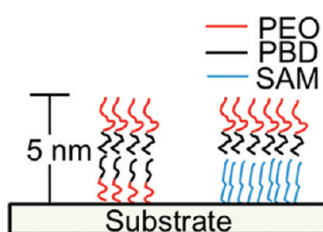


Figure 5. Schematic representation of the conformation of PEO-*b*-PBD chains on a hydrophilic substrate (left) and hydrophobic silane SAM (right). Micelles of PEO-*b*-PBD are found to deposit as either bilayers or monolayers, depending upon substrate surface chemistry.

Similar to our treatment of polymer micelle depositions on uniform surfaces, fluorescent dyes were incorporated into PEO-*b*-PBD films deposited onto SAM stamped surfaces. Figure 7 shows fluorescence microscopy images of micelle depositions with addition of fluorescent lipids (A–C) and fluorescein-labeled PEO-*b*-PBD (D). Fluidity measurements made by FRAP of the area marked by the red square allows us to probe diffusion at the interface of polymer monolayers and bilayers. We observe fluidity of only the polymer monolayers on the hydrophobic stamped squares. Bilayers that make up the grid pattern display no recovery at time scale up to 1 h. Photobleaching a single corner composed of  $\sim 1/4$  the total area of a monolayer square showed recovery in the form of a uniform square region with overall reduced fluorescence intensity. This is interpreted as indication of no mixing/fluidity at the boundary between monolayers/bilayers. Recovery is therefore limited to the dye located inside the square regions.

While similar diffusion characteristics are observed for both lipid dyes and self-labeled polymer, comparison of Figure 7A,D shows significant differences between the two labeling methods on a patterned surface. We expect that, assuming equal incorporation of dye and after subtraction of camera dark counts, bilayers should have twice the fluorescence intensity as monolayers. When the polymer is self-labeled with fluorescein, the intensity profile in Figure 7E shows this is, in fact, what we observe. In contrast, when a  $C_{12}$ -Bodipy-PC lipid-based dye is used, monolayers and bilayers produce the same intensity. Also striking is the observation that the monolayer square areas were surrounded by a dark boundary at the interface with the bilayer grid. Similar fluorescence dye behavior was obtained when the tail-labeled  $C_{12}$ -Bodipy-PC was switched to a headgroup-labeled Texas Red DHPE

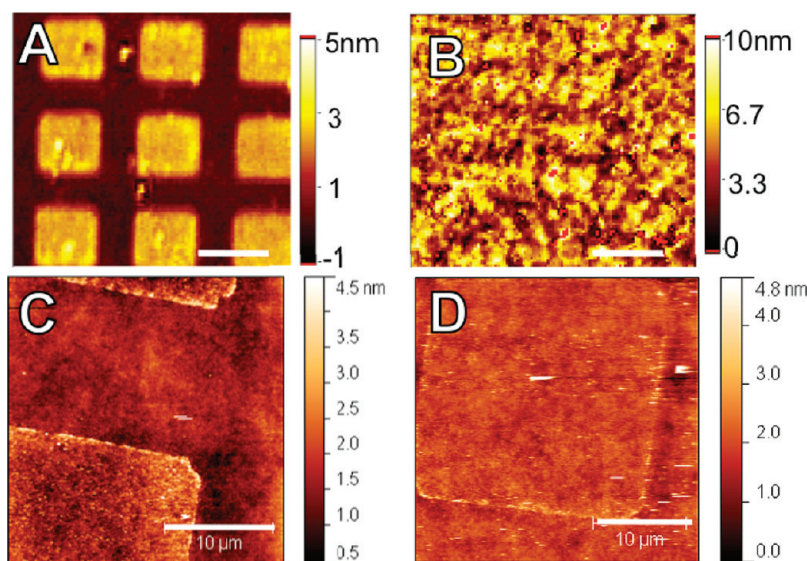


Figure 6. Scanning ellipsometry (A,B) and AFM (C,D) images of microcontact printing stamped surfaces before (A,C) and after (B,D) exposure to PEO-*b*-PBD micelles. Scale bar represents  $20 \mu\text{m}$  (A,B) and  $10 \mu\text{m}$  (C,D).

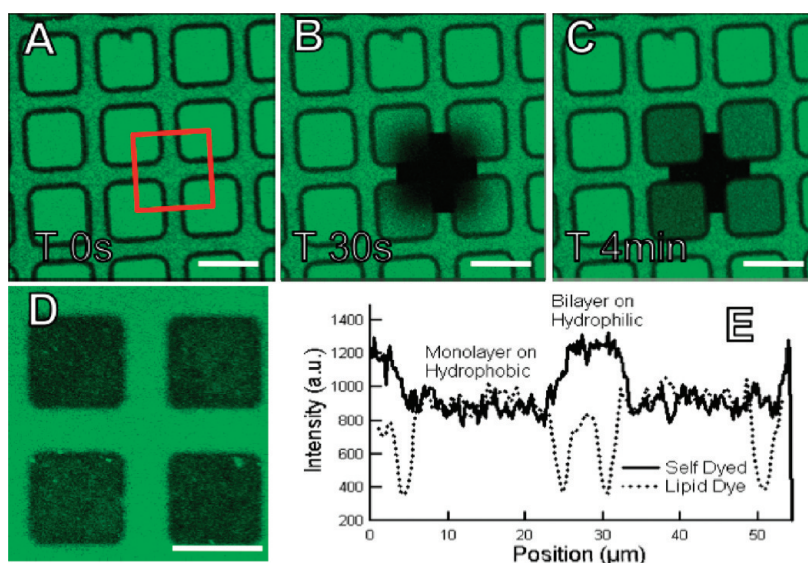


Figure 7. Fluorescence microscopy images of PEO-*b*-PBD micelles deposited on a microcontact printed glass substrate. Square regions were stamped with a hydrophobic SAM. Images show micelles labeled with C<sub>12</sub>-Bodipy-PC (A–C) and covalent attachment to fluorescein (D). A fluorescence intensity profile across two stamped squares is shown panel E. All scale bars represent 20 μm.

dye. Regardless of the specific dye used, the partitioning of small molecule dyes into PEO-*b*-PBD can be explained through previous observations of supported lipid bilayers on patterned surfaces. First, the boundary between monolayers and bilayers that is devoid of fluorescence is due to exclusion of small molecule dyes at the edge of bilayer patches. This exclusion results from an increase in intramolecular conformational order that occurs at the boundary of surfactant bilayers.<sup>29</sup> Second, the equal fluorescence intensity of monolayer and bilayers suggests that lipid-based dyes are not fully incorporated to PEO-*b*-PBD films. It is likely that dyes preferentially partition into the top polymer bilayer leaflet. This mechanism has been previously observed in solid-supported lipid bilayers and attributed to electrostatic-induced reorganization of negatively charged membrane components into the top leaflet of the bilayer.<sup>28</sup> This phenomenon may be occurring in our system since the neutral pH's of both dyes used in our study have an overall negative charge.<sup>30</sup>

The lack of fluidity in PEO-*b*-PBD bilayers, as compared to monolayers, may have several origins. While diffusion of polymer chains in bulk melts makes up a great deal of work in polymer physics, diffusion of polymers adsorbed at a solid/liquid interface is a relatively unexplored phenomenon. Initial work by the Granick lab into polymer surface diffusion has found strong dependence on both polymer/substrate and polymer/polymer interactions.<sup>31,32</sup> Coupling of polymers in bilayer and monolayer films can take the form of in-plane entanglements and interdigitation/entanglements between two leaflets. We can rule out in-plane entanglements as a diffusion barrier due to the observation that PEO-*b*-PBD monolayers display significant fluidity. Since a bilayer is simply two

monolayers with inversion symmetry, in-plane entanglements present in a bilayer would also be present in monolayers. Further evidence against entanglements comes from our choice of MW, which is below the critical entanglement length for both blocks.<sup>33</sup> Note that even if the polymers are long enough to entangle, previous studies have indicated that polymers under confinement in monolayers or bilayers lack the same reptation that is observed in bulk systems.<sup>34</sup> Another type of polymer/polymer interaction is coupling between bilayer leaflets, which in our experiment would take the form of overlapping and mixing of PBD blocks that create the hydrophobic bilayer core. Coupling between leaflets of amphiphile bilayers is a well-known phenomenon in biophysics. In the case of lipid bilayers, both in bubble-like liposomes and in solid-supported films, it is known that interleaflet coupling affects phase separation, domain registry, and transitions between liquid crystal phases.<sup>35–38</sup> While interdigitation between bilayer leaflets does not affect lateral fluidity,<sup>39</sup> interleaflet entanglements do.<sup>33</sup> If the entanglement dynamics are sufficiently long-lived relative to the diffusion time scale, two opposing and entangled molecules should diffuse together as if permanently linked. Therefore, if the proximal leaflet of a bilayer is immobile and strongly coupled to the distal leaflet, the entire bilayer will lack fluidity. If interleaflet coupling is responsible for the lack of fluidity observed in PEO-*b*-PBD, what causes the bottom leaflet to become immobile?

Besides polymer/polymer interactions, coupling of an adsorbed polymer to a solid substrate may have profound influence on the membrane fluidity.<sup>31,32</sup> Mechanical coupling of a polymer to a substrate occurs through the same intermolecular forces that cause micelle adsorption to occur. The total interaction is

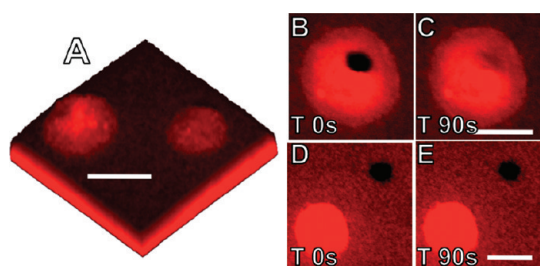


**Figure 8.** Scanning confocal fluorescence microscopy images taken during rehydration of a PEO-*b*-PBD multilamellar film. A 3D reconstruction of a 30  $\mu\text{m}$  thick *z*-stack (A) shows the growth of hollow cap structures. FRAP measurements on a cap (B,C) and on the underlying film (D,E) are also shown. Images taken immediately after photobleaching (B,D) and after 90 s (C,E) indicate that only the cap structure exhibits lateral fluidity. All scale bars indicate 20  $\mu\text{m}$ . Tetramethylrhodamine-5-carbonyl azide conjugated to the polymer was used as a fluorescent label.

determined by the strength of force, which varies significantly for contributions such as van der Waals and electrostatics, and by the amount of polymer in contact with the substrate. The latter of these is primarily determined by the conformation of the polymer chains. Similar to our work, the aforementioned studies by the Granick lab investigated the diffusion of PEO homopolymer on hydrophobic and hydrophilic silica.<sup>32</sup> They also found that adsorbed PEO displayed fluidity only on hydrophobic surfaces. While no explanation was given for this observation, we believe it is due to strong coupling from hydrogen bonding between silanol groups and PEO blocks. Note that in Granick's work PEO was observed to form monolayers that lie flat against the substrate, most likely having a greater contact area with the substrate than in our experiments. We can combine the interactions of PEO-*b*-PBD with the substrate and with itself to explain the lack of fluidity in bilayers. First, the relatively strong hydrogen bonding between PEO and hydrophilic silica causes the proximal leaflet to become immobile. Second, coupling between PBD blocks causes both leaflets to effectively diffuse at the same rate, which in this case is effectively zero.

The influence of polymer/substrate interactions on fluidity was tested by separating and decoupling a PEO-*b*-PBD film from a glass substrate through rehydration. Thin film rehydration is an often used method to produce polymer vesicles;<sup>2</sup> however, as noted previously, our choice of PEO-*b*-PBD MW tends to produce micelles instead of vesicles. Interestingly, using confocal fluorescence microscopy, we observe that rehydration produces growth of hollow hemispherical caps protruding from the remaining film. Figure 8A shows a

3D reconstruction of a multilamellar PEO-*b*-PBD film undergoing rehydration and growth of two cap structures. These caps grow over the course of several hours and remain stable and attached to the surface for days. The use of confocal microscopy to perform FRAP experiments allows for diffusion measurements of either the protruding cap (Figure 8B,C) or the underlying film (Figure 8D,E). We observe that, upon rehydration, decoupling of the PEO-*b*-PBD from the substrate creates a fluid film, while the remaining surface-bound polymer remains immobile. This supports our hypothesis of polymer/substrate interactions and interleaflet coupling limiting the fluidity of PEO-*b*-PBD bilayers.

## CONCLUSION

For the first time, the lateral diffusion characteristics of solid-supported block copolymer membranes has been studied. We demonstrate that, dependent upon surface chemistry, PEO-*b*-PBD micelles adsorb to solid surfaces to create either bilayers or monolayers. Both types of films are observed to be smooth and defect-free over hundreds of square micrometers. The fluidity of solid-supported copolymer membranes depends strongly on the interaction of the substrate and the contacting polymer block. Relatively strong hydrogen bonding creates immobile bilayers, while weaker van der Waals allows for fluidity in monolayers. Similar diffusion characteristics are measured using both fluorescent dyes conjugated directly to polymers and using lipid-based dyes as reporters. However, using soft lithography to define patterns of varying surface hydrophobicity, we observe that the partitioning of lipid-based dyes is sensitive to several variables.

We estimate that phase separation between polymer blocks produces the same hydrophilic/hydrophobic/hydrophilic structure found in natural membranes and lipid bilayers. This fundamental work serves as a starting point for challenges related to using block copolymer membranes to create nanocomposite materials. If such a composite material is to demonstrate lateral mobility and dynamic behavior, solid-supported bilayer assemblies as currently designed may not prove to be useful. Instead, new design parameters that limit entanglement effects in block copolymer synthesis will have to be investigated. The potential benefits of using polymers as organizing scaffolds makes it necessary to understand dynamics and mechanics of current designs toward the development of predictive polymer biomimetic assemblies.

## EXPERIMENTAL SECTION

All materials were used as received without further purification. Hydroxyl-terminated poly(ethylene oxide)-*block*-poly(butadiene) with block weights of 1.3 and 1.2 kDa and a polydispersity index of 1.1 was purchased from Polymer Source. Fluorescent labeling

was accomplished through addition of lipid-based dyes 2-(4,4-difluoro-5,7-dimethyl-4-bora-3a,4a-diaza-*s*-indacene-3-dodecanoyl)-1-hexadecanoyl-*sn*-glycero-3-phosphocholine ( $\text{C}_{12}$ -Bodipy-PC) and Texas Red 1,2-dihexadecanoyl-*sn*-glycero-3-phosphoethanolamine, triethylammonium salt (Texas Red DHPE) (Molecular

Probes) or by conjugating directly to the polymer. Fluorescein-5-carbonyl azide diacetate and tetramethylrhodamine-5-carbonyl azide (Molecular Probes) was used to label the hydroxyl terminus of the polymer by reacting in anhydrous chloroform for 8 h under reflux. Fluorescein-5-carbonyl azide diacetate was activated with aqueous hydroxyl amine. Unreacted dye was removed by dialysis against water for 3 days. In all cases, dyes were introduced into micelles at concentrations of  $\leq 10$  mol % to avoid self-quenching.

Micelles were prepared first by dissolving PEO-*b*-PBD in chloroform, a good solvent for both copolymer blocks. Aqueous solutions were formed by evaporation of chloroform followed by rehydrating in deionized water. In order to increase the rate of hydration and micelle formation, samples were subjected to three freeze–thaw cycles. After this treatment, the polymer was observed to be a viscous plug that did not fully dissolve after several hours. Bath sonication in ice water was used to further dissolve the polymer and create micelles. Micelles were typically created in a 1–20 mg/mL solution and stored at 4 °C until use. Dynamic light scattering (DLS) was used to characterize the size distribution of a 20 mg/mL solution and was performed using a Nanotracer instrument (Microtrac, Inc.), averaging 10 runs of 60 s each. The cloud point of micelle solutions was analyzed with an automatic melting point system (Optimelt MPA100, Stanford Research Systems). Capillary tubes were filled with 20 mg/mL solutions and were placed in the instrument, and the temperature was raised at 5 °C/min while monitoring the sample turbidity.

Depositions of micelles were investigated on three types of surfaces: hydrophilic, hydrophobic, and patterned with regions of both surface chemistries. Hydrophilic glass and silicon samples were obtained by first rinsing them in ethanol and deionized water. Samples were then cleaned in a solution of 3:1 H<sub>2</sub>SO<sub>4</sub>/30% H<sub>2</sub>O<sub>2</sub> and rinsed in deionized water. Hydrophobic samples were prepared by exposing cleaned hydrophilic substrates to vapor phase silanization with octyldimethylmethoxysilane (Gelest). Freshly cleaned samples were placed in a sealed vessel with a drop of silane and heated to 100 °C for 1 h. Unbound silanes were removed through bath sonication in ethanol. Microcontact printing was used to produce surfaces having both hydrophilic and hydrophobic regions. Briefly, a polydimethylsiloxane (PDMS) stamp was used to print a 0.4% solution of octadecyltrichlorosilane (Gelest) in dry toluene onto freshly cleaned glass slides. Stamps were wet with the silane solution, and excess was removed by blow-drying with nitrogen. Patterning was performed by holding a freshly cleaned substrate and stamp with firm pressure for 15 s. Samples were subsequently cleaned by successive bath sonication in toluene, dichloromethane, and ethanol.

Block copolymer depositions were performed by placing 50  $\mu$ L of micelle solution and 550  $\mu$ L of deionized water above surfaces and incubating at room temperature for  $\sim 20$  min. Samples were then rinsed 10 times with 400  $\mu$ L of deionized water. Care was taken to never fully dry the samples during deposition and characterization.

Polymer depositions were characterized while immersed in water through a combination quartz crystal microbalance, atomic force microscopy (AFM), laser scanning confocal microscopy, and scanning ellipsometry. Quartz crystal microbalance (QCM) experiments were conducted with a D300 instrument from Q-sense. Borosilicate glass-coated sensors were also purchased from Q-sense for both hydrophilic and hydrophobic surfaces. Hydrophilic surfaces were created by UV cleaning for 20 min, and hydrophobic surfaces were created with the vapor phase silanization reaction previously described. Changes to the third harmonic of the sensor's resonant frequency were used to monitor the kinetics of adsorption. Atomic force microscopy used a Molecular Imaging (now Agilent Technologies) Picoscan 2500 in AC (tapping) mode. AFM cantilevers (PPP-NCLR, resonant frequency  $\sim 76$  kHz in water) were purchased from Nanosensors. Imaging was done at the lowest possible set point to enhance image quality and minimize sample damage. Scratching experiments were performed by first using contact mode imaging at the highest possible set point (10 V) to remove the polymer film. The removed portion of the film was then visualized by zooming out and reimaging in AC (tapping) mode.

Laser scanning confocal microscopy used an Olympus FV-1000 microscope with a 20 $\times$  objective. Fluorescence recovery after photobleaching (FRAP) was used to measure diffusion constants of polymer membranes. Samples were first bleached using the full laser intensity and then imaged using  $\sim 5\%$  of the full intensity. Measurements were performed in triplicate, and diffusion constants were extracted using the fitting method of Kappel and Eils.<sup>21</sup> Scanning ellipsometry utilized a Nanofilm EP3-SW ellipsometer with a wavelength of 532 nm and 60° angle of incidence. Modeling of ellipsometry was performed using software provided by Nanofilm, assuming an index of refraction of 1.5 for PEO-*b*-PBD.<sup>40</sup>

**Acknowledgment.** This work was performed, in part, at the Center for Integrated Nanotechnologies, a U.S. Department of Energy, Office of Basic Energy Sciences user facility. Los Alamos National Laboratory, an affirmative action equal opportunity employer, is operated by Los Alamos National Security, LLC, for the National Nuclear Security Administration of the U.S. Department of Energy under contract DE-AC52-06NA25396.

**Supporting Information Available:** Further AFM images of PEO-*b*-PBD bilayers deposited on hydrophilic glass substrates. This material is available free of charge via the Internet at <http://pubs.acs.org>.

## REFERENCES AND NOTES

- Martin, D. K. *Nanobiotechnology of Biomimetic Membranes*, 1st ed.; Springer: New York, 2006; Vol. 1, p 182.
- Discher, D. E.; Ahmed, F. *Polymersomes*. *Annu. Rev. Biomed. Eng.* **2006**, *8*, 323–341.
- Meier, W.; Egli, S.; Nussbaumer, M. G.; Balasubramanian, V.; Chami, M.; Bruns, N.; Palivan, C. Biocompatible Functionalization of Polymersome Surfaces: A New Approach to Surface Immobilization and Cell Targeting Using Polymersomes. *J. Am. Chem. Soc.* **2011**, *133*, 4476–4483.
- Meier, W.; Onaca, O.; Enea, R.; Hughes, D. W. Stimuli-Responsive Polymersomes as Nanocarriers for Drug and Gene Delivery. *Macromol. Biosci.* **2009**, *9*, 129–139.
- Riess, G. Micellization of Block Copolymers. *Prog. Polym. Sci.* **2003**, *28*, 1107–1170.
- Belegriou, S.; Dorn, J.; Kreiter, M.; Kita-Tokarczyk, K.; Sinner, E. K.; Meier, W. Biomimetic Supported Membranes from Amphiphilic Block Copolymers. *Soft Matter* **2010**, *6*, 179–186.
- Belegriou, S.; Menon, S.; Dobrunz, D.; Meier, W. Solid-Supported Polymer Membranes. *Soft Matter* **2011**, *7*, 2202–2210.
- Dorn, J.; Belegriou, S.; Kreiter, M.; Sinner, E. K.; Meier, W. Planar Block Copolymer Membranes by Vesicle Spreading. *Macromol. Biosci.* **2011**, *11*, 514–525.
- Rakhmatullina, E.; Meier, W. Solid-Supported Block Copolymer Membranes through Interfacial Adsorption of Charged Block Copolymer Vesicles. *Langmuir* **2008**, *24*, 6254–6261.
- Gonzalez-Perez, A.; Castelletto, V.; Hamley, I. W.; Taboada, P. Biomimetic Triblock Copolymer Membranes: From Aqueous Solutions to Solid Supports. *Soft Matter* **2011**, *7*, 1129–1138.
- Rodenhausen, K. B.; Guericke, M.; Sarkar, A.; Hofmann, T.; Ianno, N.; Schubert, M.; Tiwald, T. E.; Solinsky, M.; Wagner, M. Micelle-Assisted Bilayer Formation of Cetyltrimethylammonium Bromide Thin Films Studied with Combinatorial Spectroscopic Ellipsometry and Quartz Crystal Microbalance Techniques. *Thin Solid Films* **2011**, *519*, 2821–2824.
- Yan, Y.; Zhou, X.; Ji, J.; Zang, G. Adsorption of Polymeric Micelles and Vesicles on a Surface Investigated by Quartz Crystal Microbalance. *J. Phys. Chem. B* **2006**, *110*, 24055–21059.
- Rutland, M. W.; Parker, J. L. Surface Forces between Silica Surfaces in Cationic Surfactant Solutions—Adsorption and Bilayer Formation at Normal and High pH. *Langmuir* **1994**, *10*, 1110–1121.

14. Nikoobakht, B.; El-Sayed, M. A. Evidence for Bilayer Assembly of Cationic Surfactants on the Surface of Gold Nanorods. *Langmuir* **2001**, *17*, 6368–6374.
15. Amiel, C.; Sikka, M.; Schneider, J. W.; Tsao, Y. H.; Tirrell, M.; Mays, J. W. Adsorption of Hydrophilic–Hydrophobic Block Copolymers on Silica from Aqueous Solutions. *Macromolecules* **1995**, *28*, 3125–3134.
16. Fleer, G. J.; Scheutjens, J. M. H. M. Block Copolymer Adsorption and Stabilization of Colloids. *Colloids Surf.* **1990**, *51*, 281–298.
17. Dalsin, J. L.; Messersmith, P. B. Bioinspired Antifouling Polymers. *Mater. Today* **2005**, *8*, 38–46.
18. Mecea, V. M. From Quartz Crystal Microbalance to Fundamental Principles of Mass Measurements. *Anal. Lett.* **2005**, *38*, 753–767.
19. Shen, L.; Guo, A.; Zhu, X. Y. Tween Surfactants: Adsorption, Self-Organization, and Protein Resistance. *Surf. Sci.* **2011**, *605*, 494–499.
20. Axelrod, D.; Koppel, D. E.; Schlessinger, J.; Elson, E.; Webb, W. W. Mobility Measurement by Analysis of Fluorescence Photobleaching Recovery Kinetics. *Biophys. J.* **1976**, *16*, 1055–1069.
21. Kappel, C.; Eils, R. Fluorescence Recovery after Photobleaching with the Leica Tcs Sp2. *reSOLUTION* **2004**, *18*, 1–12.
22. Tirrell, M. Block Copolymer Self-Assembly at Surfaces: Structure and Properties. In *Solvents and Self-Organization of Polymer*; Webber, S. E., Munk, P., Tuzar, Z., Eds.; Kluwer Academic: Dordrecht, The Netherlands, 1996; Vol. 327, pp 281–308.
23. Zhang, M. Q.; Desai, T.; Ferrari, M. Proteins and Cells on PEG Immobilized Silicon Surfaces. *Biomaterials* **1998**, *19*, 953–960.
24. Bayerl, T. M.; Bloom, M. Physical-Properties of Single Phospholipid Bilayers Adsorbed to Micro Glass Beads: A New Vesicular Model System Studied by H-2-Nuclear Magnetic Resonance. *Biophys. J.* **1990**, *58*, 357–362.
25. Johnson, S. J.; Bayerl, T. M.; Mcdermott, D. C.; Adam, G. W.; Rennie, A. R.; Thomas, R. K.; Sackmann, E. Structure of an Adsorbed Dimyristoylphosphatidylcholine Bilayer Measured with Specular Reflection of Neutrons. *Biophys. J.* **1991**, *59*, 289–294.
26. Koenig, B. W.; Kruger, S.; Orts, W. J.; Majkrzak, C. F.; Berk, N. F.; Silverton, J. V.; Gawrisch, K. Neutron Reflectivity and Atomic Force Microscopy Studies of a Lipid Bilayer in Water Adsorbed to the Surface of a Silicon Single Crystal. *Langmuir* **1996**, *12*, 1343–1350.
27. Lenz, P.; Ajo-Franklin, C. M.; Boxer, S. G. Patterned Supported Lipid Bilayers and Monolayers on Poly(dimethylsiloxane). *Langmuir* **2004**, *20*, 11092–11099.
28. Shreve, A. P.; Howland, M. C.; Sapuri-Butti, A. R.; Allen, T. W.; Parikh, A. N. Evidence for Leaflet-Dependent Redistribution of Charged Molecules in Fluid Supported Phospholipid Bilayers. *Langmuir* **2008**, *24*, 13250–13253.
29. Smith, A. M.; Vinchurkar, M.; Gronbeck-Jensen, N.; Parikh, A. N. Order at the Edge of the Bilayer: Membrane Remodeling at the Edge of a Planar Supported Bilayer Is Accompanied by a Localized Phase Change. *J. Am. Chem. Soc.* **2010**, *132*, 9320–9327.
30. Zimmermann, R.; Kuttner, D.; Renner, L.; Kaufmann, M.; Zitzmann, J.; Muller, M.; Werner, C. Charging and Structure of Zwitterionic Supported Bilayer Lipid Membranes Studied by Streaming Current Measurements, Fluorescence Microscopy, and Attenuated Total Reflection Fourier Transform Infrared Spectroscopy. *Biointerphases* **2009**, *4*, 1–6.
31. Zhao, J.; Granick, S. Polymer Lateral Diffusion at the Solid–Liquid Interface. *J. Am. Chem. Soc.* **2004**, *126*, 6242–6243.
32. Zhao, J.; Granick, S. How Polymer Surface Diffusion Depends on Surface Coverage. *Macromolecules* **2007**, *40*, 1243–1247.
33. Lee, J. C.-M.; Santore, M.; Bates, F. S.; Discher, D. E. From Membranes to Melts, Rouse to Reptation: Diffusion in Polymersome vs Lipid Bilayer. *Macromolecules* **2002**, *35*, 323–326.
34. Srivastava, S.; Basu, J. K. Absence of Reptation in Highly Confined Polymers. *J. Chem. Phys.* **2009**, 130.
35. Collins, M. D. Interleaflet Coupling Mechanisms in Bilayers of Lipids and Cholesterol. *Biophys. J.* **2008**, *94*, L32–L34.
36. Schick, M.; Putzel, G. G.; Uline, M. J.; Szleifer, I. Inter Leaflet Coupling and Domain Registry in Phase-Separated Lipid Bilayers. *Biophys. J.* **2011**, *100*, 996–1004.
37. May, S.; Wagner, A. J.; Loew, S. Influence of Monolayer–Monolayer Coupling on the Phase Behavior of a Fluid Lipid Bilayer. *Biophys. J.* **2007**, *93*, 4268–4277.
38. Stottrup, B. L.; Veatch, S. L.; Keller, S. L. Nonequilibrium Behavior in Supported Lipid Membranes Containing Cholesterol. *Biophys. J.* **2004**, *86*, 2942–2950.
39. Schram, V.; Thompson, T. E. Interdigitation Does Not Affect Translational Diffusion of Lipids in Liquid Crystalline Bilayers. *Biophys. J.* **1995**, *69*, 2517–2520.
40. Mark, J. E. *Polymer Data Handbook*; Oxford University Press: New York, 1999; p 1018.